RAC1 Regulates Shh-Medulloblastoma Growth via GLI-Mediated Transcription

Nitish Jangde[1], Mi Hye Lee[1], Luz Ruiz[1], Isabelle Egan[1], Anna M. Jermakowicz[1], Daniel Wynn[1], Erik Goka[2], Marc Lippman[1], David J. Robbins[1], Nagi G. Ayad[1,3]

1. Lombardi Comprehensive Cancer Center, Georgetown University Medical Center, Georgetown University, Washington D.C.
2. Revere Pharmaceuticals, 9276 Scranton Rd. Suite 500 San Diego, CA 9212
3. To whom correspondence should be addressed, na853@georgetown.edu

Abstract

Medulloblastoma (MB) is the most common malignant primary pediatric brain tumor. Current therapies are ineffective for targeting proliferation, leptomeningeal migration, and metastasis of MB cancer cells to visceral organs and therefore, novel treatments are needed. The small GTPase, RAC1, has emerged as an important regulator of actin cytoskeletal dynamics, proliferation, and migration in several cancers. However, it has not been characterized in MB and no clinical drug candidates have been described for RAC1 in MB. Here we demonstrate that RAC1 levels are higher in MB tissue relative to normal cerebellum. Further, RAC1 depletion significantly reduces proliferation and migration of Shh-MB cells *in vitro*. Mechanistically, RAC1 controls the mRNA and protein levels of the main transcription factors in the Shh pathway, GLI1 and GLI2. RAC1 binds to the GLI1 promoter highlighting a novel role in transcriptional regulation in Shh-dependent cancers. We demonstrate that the RAC1 inhibitor, GYS32661, is brain penetrant, and reduces MB growth and increases mouse survival in an orthotopic model of Shh-MB. Importantly, GYS32661 is a non-toxic clinical candidate, suggesting that it may be a novel potential drug for the treatment of either the pediatric or adult forms of MB. Collectively, our studies identify RAC1 as a druggable target in Shh-dependent MB.

Introduction

Medulloblastoma (MB) is the most prevalent malignant primary brain tumor in children, and a leading cause of childhood cancer-related illness and death(1). Current treatment strategies involve surgery, radiation (for children older than three years old), and chemotherapy(2). MB is categorized into four distinct molecular subgroups: Wingless (Wnt), Sonic Hedgehog (Shh), Group 3, and Group 4. The Shh subgroup is complex, affecting patients across a wide age range—from infants to adults—and is further subdivided into four subtypes: Shh-α (adolescents), Shh-β (infants with a poor prognosis), Shh-γ (infants with a favorable prognosis), and Shh-δ (adults)(3). It accounts for approximately 30% of all medulloblastomas, and five-year survival is about 70% for Shh-MB patients[30]. Shh-MB most frequently occurs in children under three years of age and above 17 years of age, with fewer cases reported in childhood and adolescence(4). It originates in the cerebellum from cerebellar granule progenitor cells with activation of the Shh pathway, where Shh dysregulation triggers Shh-MB tumor growth during embryonic brain development (5, 6). For example, mutations of receptors in the Shh pathway, PTCH1 and SMO (Smoothened), are often associated with Shh-MB development(7). In terms of therapeutic interventions that have been tried, SMO antagonists as well as inhibitors of the downstream transcriptional regulators of the pathway GLI1 and GLI2(8–11) have been reported. However, resistance has been observed in both preclinical and clinical settings, suggesting the need for novel therapeutic strategies(12–15).

Ras-related C3 botulinum toxin substrate 1 (RAC1) overexpression has been implicated in several cancers, such as breast cancer, non-small cell lung cancer, and head and neck

73 squamous cell carcinomas(16–18). Emerging evidence suggests that RAC1 may be a
74 therapeutic target in cancer due to its involvement in various cellular processes(19–23).
75 Our study uncovers a new mechanism in which RAC1 controls the levels of several
76 mediators of the Shh pathway, including GLI1. RAC1 depletion or inhibition reduces the
77 transcription of *GLI1*, *GLI2*, and various transcriptional and epigenetic regulators involved
78 in Shh signaling. Consistent with this finding, RAC1 inhibition with the brain penetrant
79 molecule GYS32661 reduces medulloblastoma growth *in vivo*. Our study describes the
80 RAC1 pathway as a point of therapeutic intervention for pediatric and adult Shh-MB.
81
82
83 **Results**
84 **RAC1 is overexpressed in medulloblastoma tumors.**
85 As RAC1 has not been extensively characterized in MB we wanted to determine its levels
86 in tumors relative to normal cerebellum. Microarray analysis from de Bont et al. 2008(24)
87 revealed that *RAC1* mRNA was significantly elevated in MB compared to normal
88 cerebellum (Figure 1A) Consistent with these findings, analysis of single-cell RNA-
89 sequencing (scRNA-seq) datasets revealed significantly elevated *RAC1* mRNA
90 expression in neoplastic MB cells (Hovestadt et al., 2013(25)) compared to non-
91 neoplastic cells (Darmanis et al. 2015(26)) (Figure 1B). To determine whether the
92 elevated expression was specific to tumor cells, we compared *RAC1* levels across
93 various non-neoplastic cell populations, including oligodendrocytes, microglia, neural,
94 endothelial and astrocytes. Even when accounting for variable expression in non-
95 neoplastic cell populations, *RAC1* expression was still most pronounced in neoplastic

96 cells (Figure 1C). As shown in Figure 1D, RAC1 protein is higher in human MB tissue
97 relative to cerebellum as judged by immunohistochemistry. In addition, RAC1 protein
98 expression was assayed in several human cancer cells, including MB. Among these, the
99 highest expression was observed in ONS76, which are adherent Shh-MB cells
100 (Supplementary Figure 1). Collectively, these studies indicate that RAC1 expression is
101 higher in MB relative to normal cerebellum and that ONS76 cells may be a good model
102 system to probe RAC1 activity *in vitro*.

103
104

105

106 **RAC1 regulates the expression of GLI1 and GLI2 and associated proteins.**

107 Since ONS76 cells showed the highest RAC1 expression among all tested cells, we
108 selected them for transfection with either siRNAs targeting *RAC1* or control. As shown in
109 Figure 2A and 2E, we achieved greater than 80% knockdown of RAC1 as measured by
110 real-time qPCR and Western blot analysis and real-time qPCR. Importantly, we observed
111 reduced GLI1 mRNA and protein when RAC1 was depleted (approximately 70%, Figure
112 2A-B and 2E). As GLI1 is a major transcription factor in the Shh pathway we sought to
113 determine whether other components of the Shh pathway also decreased. Indeed, when
114 we analyzed another transcriptional activator in the Shh pathway, GLI2, it was similarly
115 decreased in *RAC1* siRNA transfected cells relative to control cells (Figure 2C and 2E).
116 Our prior studies described a novel complex of GLI1, GLI2, and the epigenetic regulators
117 DNMT1 and UHRF1(27). Both DNMT1 and UHRF1 are required for Shh signaling and
118 therefore we hypothesized that RAC1 may also control their transcription and protein
119 levels. Indeed, RAC1 siRNA transfected ONS-76 cells had reduced levels of DNMT1 and

120 UHRF1 mRNA and protein (Figure 2D-E). These studies suggest that RAC1 regulates
121 the Shh pathway in MB cells by controlling the expression levels of *GLI1*, *GLI2*, *DNMT1,*
122 and *UHRF1*.
123
124 **The RAC1 inhibitor GYS32661 reduces levels of GLI1 and GLI2 *in vitro.***
125 To complement the *RAC1* knockdown studies in Shh-MB, we assessed the effect of
126 pharmacological inhibition of RAC1 in ONS76 cells. We selected the recently reported
127 RAC inhibitor GYS32661(28–31) as our studies demonstrated that it is safe and non-toxic
128 in animals and is brain penetrant (Supplementary Figure S2 and S3). We treated ONS76
129 cells with varying concentrations of GYS32661 and assessed RAC1 activity (measured
130 as GTP-bound RAC1) using GTP-RAC1 affinity-based purification followed by RAC1
131 immunoblotting. GYS32661 reduced levels of GTP-RAC1 in ONS76 cells, suggesting that
132 it effectively inhibits RAC1 activity in Shh-MB cells (Figure 3A).
133 We next evaluated the downstream effects of RAC1 inhibition on Shh signaling.
134 GYS32661 treatment led to a reduction in GLI1 and GLI2 levels in ONS76 cells (Figure
135 3B and 3C). Further, GYS32661 reduced Gli1 and Gli2 levels in a model of Shh-MB
136 derived from *Ptch1* knockout mouse tumors (*Ptch1*$^{-/-}$; MSC4 cells), suggesting that this
137 compound can broadly affect Shh-MB cells (Figure 3E and 3F). At the transcriptional
138 level, GYS32661 significantly reduced GLI1 mRNA expression in ONS76 cells (Figure
139 3G). Consistent with this, GYS32661 treatment decreased mRNA levels of *Gli1, Gli2,*
140 *Dnmt1* and *Uhrf1* in MSC4 cells (Supplementary Figure S4A).
141 Prior studies in other cancers suggested that RAC1 can function within a transcriptional
142 complex(32–35), and therefore we wanted to determine whether RAC1 controls *GLI1*

143 levels by binding to chromatin in Shh-MB. To assess this, we performed a Chromatin
144 Immunoprecipitation assay (ChIP) in ONS76 cells to determine whether RAC1 is localized
145 to the *GLI1* promoter. We found that RAC1 binds to a previously characterized *GLI1*
146 promoter region in ONS76 cells (-4230/-4424 *GLI1* upstream, Figure 3I). Among three
147 different regions, the upstream -4230/-4424 showed significantly higher fold enrichment
148 as compared to the IgG control, which suggests that RAC1 binds to this region.
149 Importantly, treatment with GYS32661 for 24 hours reduced RAC1 binding to this region
150 as compared to the DMSO control (Figure 3H-I). Collectively, these studies suggest that
151 RAC1 directly controls *GLI1* transcription by binding to its promoter.
152
153
154 **GYS32661 treatment reduces levels of GLI1-UHRF1-DNMT1 complex *in vitro***
155 Our prior studies demonstrated that the FDA-approved DNMT1 inhibitor 5-azacytidine,
156 disrupts the GLI-UHRF1-DNMT1 complex, and dramatically reduces Shh-MB growth *in*
157 *vivo*(27). Therefore, pharmacological targeting of this complex is feasible, which
158 motivated us to test whether GYS32661 would similarly affect the GLI-UHRF1-DNMT1
159 complex. We treated ONS76 or MSC4 cells with GYS32661 and measured the steady-
160 state levels of the mRNA and protein of all the components of the GLI-UHRF1-DNMT1
161 complex. As shown in Figure 3A-G, GYS32661 treatment reduced the levels of all
162 components of this complex.
163
164 As an independent test, we also checked the interactions of the GLI-UHRF1-DNMT1
165 complex using an immunofluorescence-based Proximity ligation assay (PLA) (Figure 4A-

166 D). GLI1-DNMT1 interaction was significantly inhibited by GYS32661 compound
167 treatment as the number of PLA puncta per nucleus showing GLI1-DNMT1 interactions
168 were significantly decreased in treated ONS76 and MSC4 cells (Figure 4A-B). Similarly,
169 GYS32661 treatment reduced GLI1-UHRF1 PLA puncta per nuclei in both ONS76 and
170 MSC4 cells (Figure 4C-D). Importantly, siRNA mediated depletion of *RAC1* in ONS76
171 cells also reduced the GLI1-GLI2 interaction by PLA in ONS76 cells (Supplementary
172 Figure S4C). Altogether, these studies suggest that RAC1 inhibition or depletion reduces
173 the steady-state levels of the components of the GLI-UHRF1-DNMT1 complex, thereby
174 diminishing their interaction in ONS76 and MSC4 cells.
175
176 **GYS32661 treatment inhibits cellular motility of ONS76 cells *in vitro*.**
177 RAC1 has been shown to have a myriad of roles in proliferation and migration of multiple
178 cell types(20, 21, 36) and therefore we wanted to first test whether RAC1 inhibition would
179 affect Shh-MB cellular migration. We first assessed the efficacy of GYS32661 treatment
180 in a wound healing assay in ONS76 cells. GYS32661 treatment resulted in a marked
181 decrease in cellular migration across the wound, thereby impairing wound healing
182 (Supplementary Figure S5A). A chemotaxis experiment was also performed to assess
183 the efficacy of the GYS32661 compound on cellular movement. ONS76 cells were
184 seeded in very low numbers and movement was tracked by time-lapse imaging in the
185 presence of GYS32661 or vehicle control. Importantly, the path length in GYS32661
186 treated cells shorter (approximately 280μm) than in control (approximately 380μm),
187 suggesting that this compound inhibited cellular migration in a chemotaxis assay
188 (Supplementary Figure S5B).

189

190 We next determined whether disrupting actin dynamics can be part of the reason for
191 reduced migration in GYS32661 cells. Actin polymerization and depolymerization is
192 essential for stress fiber formation, lamellipodia, filopodia, and membrane ruffling, which
193 facilitate cellular motility or migration. The Rho GTPases RhoA, RAC1, and CDC42 are
194 well recognized as critical regulators of actin dynamics and membrane structures (22, 23,
195 37, 38). To determine the effect of GYS32661 on actin polymerization, ONS76 cells were
196 treated with GYS32661 or DMSO control, then stained with Phalloidin (Alexa Fluor 488;
197 Green) or DAPI (Blue). The results showed a significant decrease in filamentous actin
198 levels after GYS32661 treatment (Supplementary Figure S6A). Interestingly, treated cells
199 had a distinct morphology compared to control cells with less stress fibers and filopodia
200 formation (Supplementary Figure S6A). Therefore, GYS32661 disrupted actin
201 cytoskeleton organization, consistent with the established roles of RAC1 in these
202 processes.

203

204 **GYS32661 treatment inhibits cellular proliferation *in vitro*.**

205 Multiple studies have shown that proliferation and migration are coupled processes(39),
206 and therefore we wanted to determine whether the effects we observe on migration of
207 ONS76 cells can also be related to proliferation inhibition following GYS32661 treatment.
208 To test this, we treated ONS76 cells with GYS32661 and performed PI-FACS analysis.
209 As seen in Supplementary Figure S6B, GYS32661 treatment arrests ONS76 cells at the
210 G1 phase of the cell cycle after 6 hours, 18 hours, and 24 hours of treatment. This is
211 consistent with the observed reduction in Cyclin D1 levels after treatment (Supplementary

212 Figure S5C and Supplementary Figure S6C), as Cyclin D1 has an established role in G1
213 progression and RAC1 has previously been implicated in controlling its levels in other
214 cancers(40). These studies suggest that RAC1 controls cell cycle progression of ONS76
215 cells.
216
217 Primary cilia formation is the hallmark of Shh-MB and its disassembly facilitates mitotic
218 division or cellular proliferation(37, 38, 41). We stained GYS32661-treated ONS76 cells
219 for acetylated tubulin and Pericentrin and we found a dramatic increase in acetylated
220 tubulin and Pericentrin positive primary cilia number in treated cells after 24 hours.
221 However, primary cilia length was not affected (Supplementary Figure S7A). Intraciliary
222 transport downstream signaling was also assessed by immunoblotting upon GYS32661
223 treatment of MSC4 cells. Vav2 and Ift88 phosphorylation was inhibited after GYS32661
224 treatment of MSC4 cells via dephosphorylation of Pak1 (Supplementary Figure S7B-C).
225 Gsk3β phosphorylation was also inhibited with increasing concentrations of GYS32661
226 treatment (Supplementary Figure S7C). In addition, acetylated tubulin (AcTub) levels
227 showed a marked increase after 18 and 24 hours of 8 μM of GYS32661 treatment while
228 Arl13b (ADP-ribosylation factor-like protein 13B) was not affected with the treatment
229 (Supplementary Figure S7D). Arl13b is a small GTPase involved in migration and intra-
230 flagellar transport (IFT) signaling(42, 43) while acetylated tubulin is an axoneme marker
231 for primary cilia also involved in intra-flagellar transport. Importantly, tubulin acetylation is
232 associated with reduced proliferation(44). Collectively, these studies suggest that
233 GYS3266's effects on ONS76 and MSC4 cells may be related to cell cycle progression
234 and signaling.

235

236

237 **GYS32661 reduces Shh-MB growth and is well-tolerated and brain penetrant *in***
238 ***vivo*.**

239 Given that GYS32661 treatment reduced proliferation of Shh-MB cells *in vitro*, we wanted
240 to determine whether it could potentially inhibit tumor growth *in vivo*. To test this, we
241 performed mice allograft experiments with MSC4 cells (Figure 5 A-D). Shh-MB tumors
242 started developing after 2 weeks, which we confirmed by MRI. We treated mice in two
243 groups: one with vehicle (normal saline; NaCl in sterile pH 9.0) and another with
244 GYS32661 (25 mg/kg body weight in sterile normal saline). The mice were treated for 3
245 weeks, and samples were collected after euthanasia and perfusion when the mice
246 showed neurological symptoms. Once mice started showing classical MB neurological
247 symptoms such as head tilting, difficulty in walking, lethargy, or ataxia, their brains were
248 scanned by MRI to detect MB tumors. GYS32661-treated mice showed a marked
249 reduction in Shh-MB tumor development compared to vehicle-treated mice (Figure 5A-
250 C). Notably, mice showed a statistically significant increase in survival upon GYS32661
251 treatment (Figure 5D).

252 Tumor tissues were collected at 3 weeks, fixed in 4% formalin and subsequently
253 embedded in paraffin. These paraffin-embedded tumor samples were sectioned and
254 stained for histological markers for proliferation (Ki67) and cell death or apoptosis markers
255 (cleaved caspase-3). GYS32661-treated tumors showed markedly reduced Ki67 staining
256 compared to vehicle-treated mice MB tumors and had higher apoptosis as judged by
257 cleaved caspase-3 (Figure 5E). GYS32661 treatment also reduced levels of on-target

258 biomarkers in the Shh pathway such as GLI1 and GLI2 *in vivo*, suggesting that the
259 compound reaches the tumor site (Figure 5F). Collectively, these studies suggest that
260 GYS32661 increases apoptosis while reducing proliferation and Shh signaling *in vivo*.
261
262 In addition to effectively reducing Shh-MB tumor burden *in vivo*, GYS32661 was well-
263 tolerated in animals. Tumor bearing mice treated with GYS32661 did not show any
264 reduction in body weight compared to untreated mice (Supplementary Figure S2A).
265 Similarly, toxicological studies in rats suggest that GYS32661 has no negative effect on
266 the body weight of either male or female rats (Supplementary Figures S2B-C). Further,
267 the dose used in our efficacy studies (25mg/kg) is well-below the maximum tolerated dose
268 tested in rats (45 mg/kg; Supplementary Figure S2B-C). To assess the effect of treatment
269 on the visceral organs, liver and brain weights were also measured in the same groups
270 of male and female rats and no observable toxicity was found (0-45 mg/kg/day for 28
271 days; Supplementary Figures S3A-D). Importantly, the compound is 50% brain penetrant
272 as determined by HPLC analysis of brain and plasma levels (Supplementary Figures
273 S3E-F). Collectively, these studies suggest that GYS32661 is brain penetrant and safe in
274 animal models.
275
276
277 **Discussion**
278 Our present study provides compelling evidence that RAC1 controls Shh-MB growth by
279 regulating GLI1 and GLI2 levels. Genetic or pharmacological inhibition of RAC1 reduced
280 GLI1 and GLI2 levels *in vitro*. In addition, GYS32661 reduced tumor growth and increased

281 survival in a mouse model of Shh-MB. It is also safe in multiple animal models.
282 Collectively, our findings demonstrate that GYS32661 is a promising treatment for Shh-
283 MB.
284
285 Our studies suggest that there is a likely therapeutic window 35mg/Kg body weight or less
286 for GYS32661 since RAC1 is expressed higher in Shh-MB tumors relative to normal brain.
287 Microarray and scRNA-seq analysis of neoplastic relative to non-neoplastic cells showed
288 high *RAC1* expression in neoplastic cells, with low expression across various non-
289 neoplastic cell types (Figure 1A-C). Further, RAC1 protein levels were higher in
290 medulloblastoma patient samples relative to normal cerebellum. Notably, RAC1 levels
291 are further increased in metastatic MB compared to non-metastatic MB, suggesting a
292 potential association with tumorigenesis and dissemination (Figure 1D). Collectively, our
293 results suggest RAC1 mRNA and protein levels are higher in neoplastic cells within
294 medulloblastoma tumors relative to normal cerebellum. These findings support the notion
295 that RAC1 plays a role in MB tumorigenesis with limited effect on non-tumor brain tissue,
296 and therefore it may represent a viable therapeutic target for Shh-MB.
297
298 Although RAC1 has been described within the context of Shh signaling, we present a new
299 model of how it affects this important pathway in Shh-MB. Prior studies focused on a
300 possible role for RAC1 in GLI1 shuttling from the cytoplasm to the nucleus(32, 33, 35,
301 45). However, we did not observe any concentration or time point where GYS32661
302 treatment affected GLI1 shuttling. Rather, under all conditions, we observed a marked
303 reduction in the total mRNA and protein levels of GLI1, GLI2, DNMT1, and UHRF1. This

304 is consistent with a role for RAC1 in transcription of these genes, supported by our
305 findings that RAC1 localizes to the *GLI1* promoter. Therefore, RAC1 may have a similar
306 role in other cancers where it acts in the nucleus to affect transcription of essential genes
307 involved in proliferation, migration, and metastasis.
308
309 Given that RAC1 plays multiple roles in different cells it is not surprising that it affects both
310 proliferation and migration of Shh-MB cells. Although it is not possible to separate the
311 effects on migration from proliferation in dividing cells, we favor a model where RAC1
312 plays a role in proliferation of Shh-MB cells. As shown in our FACS analysis, RAC1
313 inhibition via GYS32661 treatment increased the percentage of cells in the G1 phase of
314 the cell cycle, reduced G2 and S phase cells, and Cyclin D1 levels (Supplementary Figure
315 S5C and Supplementary Figure S6B-C). This suggests that RAC1 inhibition regulated
316 cell cycle progression, which is consistent with its role in different other cancers(33, 46).
317 Our data suggest that RAC1's effects on the cell cycle are at least in part due to RAC1
318 binding to the *GLI1* promoter and affecting *GLI1* transcription, although we acknowledge
319 it is difficult to separate its multiple roles in the cell cycle.
320
321 The effects of RAC1 on proliferation can also be related to primary cilia dysfunction, as
322 suggested by other studies(19, 47–49). However, our analysis of GYS32661-treated cells
323 did not indicate a change in the length of primary cilia (Supplementary File S6A). We
324 further noted that treatment with GYS32661 increased α-tubulin acetylation substantially,
325 which is associated with changes in proliferation based on prior studies. By contrast,
326 GYS32661 did not affect Arl13b accumulation, which is associated with longer cilia in

327 other studies(50). Therefore, the effect of GYS32661 on primary cilia number is likely
328 related to its ability to inhibit the cell cycle in ONS76 cells.
329
330 Our studies suggest that targeting Shh-MB via inhibiting RAC1 with GYS32661 is a novel
331 means of downregulating GLI1, GLI2, UHRF1, and DNMT1 activity. This indicates GLI
332 proteins as potential druggable targets to treat medulloblastoma patients. Recently, an
333 epigenetic regulatory complex, GLI-UHRF1-DNMT1, has been found to be a key regulator
334 and druggable target of Shh-MB(27). In a genome-wide CRISPR-Cas9 knockout
335 screening of human (DAOY) and murine (SMB21) Shh-MB cells, DNMT1 has been
336 identified as an epigenetic regulator and a potential target for monotherapy(51). Normal
337 cerebellar development and Shh-MB expansion depend on DNMT1. Targeting Shh
338 signaling downstream of SMO, either through its pharmacological inhibition alone or in
339 conjunction with SMO inhibitors, effectively restricts tumor development and increases
340 survival in Shh-MB models(52–54).
341
342 UHRF1 is a key regulator of DNA methylation in mammalian cells. Research has also
343 indicated that UHRF1 contributes to the development of tumors (55–57). In a recent
344 study, immunostaining and western blotting analysis of sixty-eight MB patients showed
345 that UHRF1 expression is present in MB tissues but absent in the normal cerebellum(57).
346 In the same study RNAi-mediated UHRF1 downregulation inhibited MB cell proliferation
347 and colony formation, induced G1/G2 cell cycle arrest, elevated p16 expression, and
348 altered CDK4 location. Altogether these results suggest that UHRF1 may be a useful

349 biomarker and treatment target for MB and therefore GYS32661's ability to decrease
350 UHRF1 levels in Shh-MB tumors is therapeutically advantageous.
351
352 Our present study identifies the crosstalk between RAC1-mediated GLI1 activity and the
353 GLI epigenetic complex-mediated GLI1 activity in Shh-MB development. This is the first
354 report of RAC1 inhibition targeting every component of the epigenetic complex (GLI1,
355 GLI2, DNMT1 and UHRF1 complex), suggesting a novel mechanism in RAC1-mediated
356 Shh-MB development. Collectively, our study suggests a novel role for RAC1 in targeting
357 the druggable GLI epigenetic complex by regulating the transcription of the components
358 of the complex, which eventually can restrict Shh-MB development (Graphical abstract)
359 GYS32661's ability to reduce on-target biomarkers in the Shh pathway in orthotopic
360 models is likely related to its considerable brain penetrance (Supplementary File S3E-F).
361 Although other RAC1 inhibitors have been described (30, 58) to our knowledge this is the
362 first time one has been demonstrated to be brain penetrant and effective in animal models
363 of Shh-MB. These studies and other drug-like characteristics of GYS32661 suggest that
364 a clinical trial should be considered for patients suffering from Shh-MB.
365
366 **METHODS**
367 *Data Analysis*
368 Medulloblastoma scRNA-seq data (neoplastic) was obtained from the Hovestadt 2013
369 and non-tumor brain cell (non-neoplastic) scRNA-seq data was obtained from the
370 Darmanis 2015 study(25, 26) Analysis and visualization of gene expression was
371 performed using the Seurat R package(59–63).Differences in gene expression between

372 neoplastic and non-neoplastic cells was performed using MAST (implemented in
373 Seurat)(64). The de Bont et al 2008(24) microarray data set was acquired from Gliovis
374 (http://gliovis.bioinfo.cnio.es/) and analyzed to compare gene expression of
375 medulloblastoma tumor to normal cerebellum(65).
376
377
378
379 *Cell culture*
380 Human Shh medulloblastoma cell line ONS76 was grown in RPMI 1640 medium (with
381 ATCC modification) with 10% Fetal bovine Serum (FBS) and 1x Anti-anti at 37°C, 5%
382 CO_2. Mouse medulloblastoma spheroid cells (MSC4) isolated from Shh MB tumors of
383 genetic conditional *Ptch1* knockout mice were grown in DMEM F12 medium with 1x B27
384 supplement at 37°C, 5% CO_2. Ptch1LoxP (B6;129T2-Ptch1tm1Bjw/ WreyJ), and Gfap-Cre
385 (FVB-Tg(GFAP-cre)25Mes/J) strains were obtained from the Jackson Laboratory and bred to
386 generate Ptch1-Gfap mice(66). Cells from spontaneous tumors in these mice were grown in
387 Dulbecco's modified Eagle's medium (DMEM)/F12 (Gibco), B27, and penicillin-streptomycin to
388 generate vismodegib-sensitive SHH-MB cultures: SHH-S47 and Ptch1-Gfap. SHH-S47 and
389 Ptch1-Gfap cells were gifted by Dr. Jezebel Rodriguez-Blanco's laboratory.
390
391 *Gene silencing experiment*
392 Cells were transfected with targeting Rac1 siRNA (SantaCruz Biotechnology; Catalog no.:
393 sc-36351) and non-targeting siRNAs (Santa Cruz Biotechnology; Catalog no.: sc-
394 370071)), transfection reagent and transfection media per the manufacturer's protocol.

395 After knockdown immunoblotting and qPCR experiments were performed for
396 confirmation.
397
398
399 *Cell lysis and immunoblotting*
400 Lysis buffer (Cell Signaling) containing protease and phosphatase inhibitors was added
401 to cells. The resulting extracts were centrifuged at 16,000 x g for 10 minutes at 4 °C to
402 collect the soluble fraction. Protein concentrations were measured by the Qubit Protein
403 Assay (Invitrogen). Subsequently, 40 µg protein of each sample was resolved on SDS-
404 PAGE, transferred on a nitrocellulose membrane, and immunoblotting was performed
405 using respective antibodies.
406
407 *RNA isolation and Quantitative Realtime PCR (qRT-PCR)*
408 Total RNA was purified and using the AllPrep DNA/RNA Mini Kit (Qiagen). Reverse
409 transcription was conducted using the SuperScript III First-Strand Synthesis SuperMix
410 (ThermoFisher). Quantitative real-time PCR (qRT-PCR) was conducted with the
411 SsoAdvanced Universal SYBR Green Supermix (Bio-Rad) and gene-specific primers
412 (Supplementary Table S1) on a CFX Opus96 Real-Time qPCR Detection System (Bio-
413 Rad). The ΔΔCt method was used with *Gapdh* or *18S* rRNA as the reference
414 (Supplementary Table S1) to calculate the fold change in gene expression.
415
416
417 *Chromatin immunoprecipitation (ChIP)*

418 ONS76 cells were cross-linked with formaldehyde, lysed, and sonicated. Chromatin was
419 immunoprecipitated with the anti-RAC1 antibody (clone 23A8, Catalog No. 05-389) or a
420 negative control normal Rabbit IgG antibody (Sigma, Catalog No. 12-370). The DNA was
421 recovered after removal of DNA–protein cross-links and subjected to quantitative
422 amplification of the primers specific to the human Gli1 locus(67) (see Supplementary
423 Table S2).
424
425 *Wound healing assay*
426 The migratory response of cells to GYS32661 was examined in a scratch assay. Cells
427 were seeded into 12-well plates (3×10^5 cells/well) and allowed to grow to 90–100%
428 confluence, then serum-starved overnight. A scratch was created using a 200 µl sterile
429 pipette tip, and PBS was used to remove cell debris. Cells were then treated with DMSO
430 control, media with 5% FBS (positive control) and media with 2 µM GYS32661 for
431 18 hours at 37 °C. Cell migration was observed using a Keyence phase contrast
432 microscope BZ-X800, and wound closure was quantified compared to untreated controls
433 by using Fiji wound healing quantification software.
434
435 *Chemotaxis assay*
436 The migratory response of cells to GYS32661was examined. Cells were seeded into 8-
437 well chambered slides (Ibidi) in 1×10^3 cells/well density and allowed them to adhere,
438 then serum-starved overnight. Cells were then treated with DMSO control, media, or with
439 2 µM GYS32661 for 12 hours at 37 °C in live cell imaging incubator chamber. Cellular

440 movement was documented by time lapse imaging on a Keyence phase BZ-X800
441 contrast microscope, and quantified by Keyence software BZ-X800.
442
443
444
445 *GTP-bound RAC1 detection*
446 Cells were treated with varying concentrations of the GYS32661 compound. Cells were
447 harvested under non-denaturing conditions by rinsing them with PBS and lysing them
448 with an ice-cold lysis solution (25mM Tris-HCl, pH 7.2, 150mM NaCl, 5mM $MgCl_2$, 1%
449 NP-40, and 5% glycerol containing PMSF), followed by incubation on ice. Cell lysates
450 were mixed with EDTA, GTPγS (positive control), or GDP (negative control) and
451 incubated at 30°C. The reaction was terminated with 1 M $MgCl_2$ (final working
452 concentration 60 mM) followed by cooling on ice for GTPγS or GDP treatment.
453 Subsequently, the treated lysates were subjected to affinity precipitation using glutathione
454 resin and GST-PAK1-PBD. After gentle shaking at 4°C, the resin was thoroughly washed
455 with lysis buffer, and the GTP-bound RAC1 protein was eluted using a reducing sample
456 buffer containing DTT. The samples were then electrophoresed and immunoblotted for
457 RAC1.
458
459 *Proximity ligation Assay (PLA)*
460 PLA was performed on cells using a Duolink Proximity Ligation Assay (Millipore Sigma)
461 as described by the manufacturer. The following antibodies were used for PLA: UHRF1
462 (catalogue no. sc-373750, Santa Cruz Biotechnology, RRID: AB_10947236), DNMT1

463 (catalogue no. 5032, Cell Signaling Technology, RRID: AB_10548197), GLI1 (catalog no.
464 AF3455, R&D Systems, RRID: AB_2247710), GLI2 (catalog no. AF3635, R&D Systems,
465 RRID: AB_2111902), rabbit IgG (catalog no. 12370, Millipore Sigma). DAPI staining was
466 performed using ProLong Gold Antifade Mountant with DAPI (Invitrogen).
467
468
469
470
471
472 *Immunofluorescence*
473 GLI1/Phalloidin immunofluorescence studies were performed on ONS76 cells after
474 GYS32661 or DMSO treatment. Spheroid cells (MSC4) were dissociated by Accutase
475 (Gibco) treatment for 5 minutes, centrifuged at 2,000 rpm for 5 minutes, and seeded at 5
476 X 10^5 density on poly-L-Lysine pre-coated coverslips (Corning) in a 24-well plate.
477 Cells were fixed with 4% PFA and permeabilized using 0.1% Triton X-100 in PBS for 15
478 minutes. 1% BSA in PBS was used to block for 45 minutes at room temperature. Slides
479 were then incubated with GLI1 antibody and fluorescent phalloidin staining solution.
480 Confocal LEICA SP8 microscopy was used to take images of cells after washing.
481 For cilia staining, cilia were counted in 4% PFA fixed cells after staining with Acetylated
482 tubulin (Sigma cat # T6793) and pericentrin (Novus Cat # NB100-61071) antibodies to
483 mark cilia and the centrosome. Acetylated tubulin-positive cilia were counted by Zeiss
484 confocal microscopy (LMS 800) and the % ciliated cells were normalized by Dapi
485 counting.

486

487 *In vivo drug dosing*

488 MSC4 spheroid cells were dissociated by passing through the 8μm cell strainer followed
489 by Accutase (Gibco) treatment. Viable cells were counted using a Cellometer followed by
490 Acridine orange/Propidium Iodide (AO/PI) staining. Orthotopically 1 X 10^5 cells/mouse
491 were injected into the cerebellum. Before injection a 0.25-inch incision was created on
492 the back of the scalp with a sterilized scalpel. A dental drill was utilized to create a
493 implanted into the cerebellum using the coordinates 2 mm down lambda, 2 mm right of
494 the midline suture, and 2 mm deep(66). The mouse was secured on a stereotactic frame
495 by mounting its incisors onto the frame hold. A 10 μL bevel-tipped syringe, which had
496 been preloaded with 4 μL of tumor cell solution, was slowly inserted into the burr hole.
497 After the bevel of the syringe needle went beneath the skull surface, it was moved an
498 additional 3 mm down before being moved up 0.5 mm. The suspension of the tumor cells
499 was slowly injected under continuous pressure over 30 seconds into the cerebellum. After
500 the injection, the needle was retained in position for two minutes before both the needle
501 and syringe were withdrawn slowly. Finally, the wound was closed using an autoclip. The
502 mice were injected intraperitoneally every other day with GYS32661 compound (35 mg/
503 Kg of body weight) in 0.9% normal saline pH 5.5 and vehicle (0.9% normal saline pH 5.5).
504 MRI imaging was performed to monitor tumor development every week. GYS32661
505 compound was also administered in different doses to male and female rats as indicated.
506 After 28 days the body, liver and brain weight of the treated rats were recorded. The brain
507 and blood plasma concentrations of GYS32661 were also measured by HPLC.

508

509 *Immunohistochemistry (IHC)*

510 The tissue samples were fixed in 10% Formalin in PBS and paraffin embedded. The
511 formalin fixed paraffin embedded (FFPE) tissues were sectioned by microtome up to
512 4 μm of thickness. Further, for immunohistochemical staining, endogenous peroxidases
513 were blocked in 3% hydrogen peroxide in methanol. These sections were probed with
514 primary antibody RAC1 Mouse Monoclonal antibody (Proteintech; Cat No. 66122-1-Ig),
515 Ki-67 (Ab15580), Cleaved Caspase-3 (Asp175) Antibody (Cell signaling technology; Cat
516 No. 9661), GLI1 Antibody (A-7) (SantaCruz Biotechnology; Cat No. sc-515781), GLI-2
517 Antibody (R & D Systems; Cat No. AF3635) and DNMT1 (D63A6) XP Rabbit mAb (Cell
518 signaling technology; Cat No. 5032) Tumor tissue sections slides were subsequently
519 incubated with VECTASTAIN® ABC-HRP Kit, Peroxidase (Mouse IgG) (PK-4002) or
520 VECTASTAIN® ABC-HRP Kit, Peroxidase (Rabbit IgG) (PK-4001) secondary antibody.
521 Staining was visualized DAB Substrate Kit, Peroxidase (HRP), with Nickel, (3,3'-
522 diaminobenzidine) (SK-4100) chromogen and counterstained with hematoxylin. The IHC
523 DAB stained images intensity were quantified as area by using ImageJ software.

524

525

526

527 **Acknowledgements**

528 We acknowledge R21NS135506, R01NS118023, and the BellRinger at Lombardi
529 Comprehensive Cancer Center of Georgetown University for funding. We also
530 acknowledge Ms. Poorna Prakash for her intensive efforts in helping with primary cilia
531 number counting and length measurement. We thank all members of the Ayad laboratory

for helpful discussions. We are grateful to Takele Yazew, our laboratory manager, for helping us during animal surgeries. We acknowledge the Shared Resource Facilities at Georgetown University including the HTSR and FACS cores.

Contribution

NJ designed and performed experiments and wrote and edited manuscript. M-H L performed experiments and edited manuscript. LR performed analysis and edited manuscript. IE performed experiments and edited manuscript. AMJ assisted with data interpretation and generated figures. ML, DW, DR, edited manuscript. NGA designed experiments and edited manuscript.

References

1. Lee B, et al. Medulloblastoma cerebrospinal fluid reveals metabolites and lipids indicative of hypoxia and cancer-specific RNAs. *Acta Neuropathol Commun*. 2022;10(1):25.

2. Bailey S, et al. Medulloblastoma therapy: Consensus treatment recommendations from SIOP-Europe and the European Reference Network. *EJC Paediatr Oncol*. 2025;5. https://doi.org/10.1016/j.ejcped.2024.100205.

3. Skowron P, et al. The transcriptional landscape of Shh medulloblastoma. *Nat Commun*. 2021;12(1):1749.

553 4. Ray S, et al. Subgroup-Specific Diagnostic, Prognostic, and Predictive Markers Influencing
554 Pediatric Medulloblastoma Treatment. *Diagnostics*. 2022;12(1).
555 https://doi.org/10.3390/diagnostics12010061.

556 5. Gibson P, et al. Subtypes of medulloblastoma have distinct developmental origins. *Nature*.
557 2010;468(7327):1095–1099.

558 6. Juraschka K, Taylor MD. Medulloblastoma in the age of molecular subgroups: a review:
559 JNSPG 75th Anniversary Invited Review Article. *J Neurosurg Pediatr PED*. 2019;24(4):353–363.

560 7. Jing J, et al. Hedgehog signaling in tissue homeostasis, cancers and targeted therapies. *Signal*
561 *Transduct Target Ther*. 2023;8(1):315.

562 8. Zeng L-H, et al. Phosphorylation of human glioma-associated oncogene 1 on Ser937 regulates
563 Sonic Hedgehog signaling in medulloblastoma. *Nat Commun*. 2024;15(1):987.

564 9. Ruppert JM, et al. The GLI-Kruppel Family of Human Genes. *Mol Cell Biol*. 1988;8(8):3104–
565 3113.

566 10. Kinzler KW, Vogelstein B. The GLI Gene Encodes a Nuclear Protein Which Binds Specific
567 Sequences in the Human Genome. *Mol Cell Biol*. 1990;10(2):634–642.

568 11. Kinzler KW, et al. Identification of an Amplified, Highly Expressed Gene in a Human Glioma.
569 *Science*. 1987;236(4797):70–73.

570 12. Harada K, et al. Hedgehog Signal Inhibitor GANT61 Inhibits the Malignant Behavior of
571 Undifferentiated Hepatocellular Carcinoma Cells by Targeting Non-Canonical GLI Signaling. *Int J*
572 *Mol Sci*. 2020;21(9). https://doi.org/10.3390/ijms21093126.

573 13. Carballo GB, et al. GANT-61 Induces Autophagy and Apoptosis in Glioblastoma Cells despite
574 their heterogeneity. *Cell Mol Neurobiol*. 2021;41(6):1227–1244.

575 14. Fu J, et al. GANT-61 inhibits pancreatic cancer stem cell growth in vitro and in
576 NOD/SCID/IL2R gamma null mice xenograft. *Cancer Lett*. 2013;330(1):22–32.

577 15. Wang J, et al. Inhibition of autophagy potentiates the efficacy of Gli inhibitor GANT-61 in
578 MYCN-amplified neuroblastoma cells. *BMC Cancer*. 2014;14(1):768.

579 16. De P, Aske JC, Dey N. RAC1 Takes the Lead in Solid Tumors. *Cells*. 2019;8(5).
580 https://doi.org/10.3390/cells8050382.

581 17. Skvortsov S, et al. Rac1 as a potential therapeutic target for chemo-radioresistant head and
582 neck squamous cell carcinomas (HNSCC). *Br J Cancer*. 2014;110(11):2677–2687.

583 18. De P, et al. Active RAC1 Promotes Tumorigenic Phenotypes and Therapy Resistance in Solid
584 Tumors. *Cancers*. 2020;12(6). https://doi.org/10.3390/cancers12061541.

585 19. Tang C, et al. Hedgehog signaling is controlled by Rac1 activity. *Theranostics*.
586 2022;12(3):1303–1320.

587 20. Schoen LF, et al. The PI3K inhibitor pictilisib and the multikinase inhibitors pazopanib and
588 sorafenib have an impact on Rac1 level and migration of medulloblastoma in vitro. *J Cell Mol*
589 *Med*. 2022;26(23):5832–5845.

590 21. Bhoopathi P, et al. SPARC mediates Src-induced disruption of actin cytoskeleton via
591 inactivation of small GTPases Rho–Rac–Cdc42. *Cell Signal*. 2011;23(12):1978–1987.

592 22. Vidal C, et al. Cdc42/Rac1-dependent activation of the p21-activated kinase (PAK) regulates
593 human platelet lamellipodia spreading: implication of the cortical-actin binding protein
594 cortactin. *Blood*. 2002;100(13):4462–4469.

595 23. Kim B, Suh YH, Joe E. LRRK2 decreases microglial actin dynamics by filamentous actin
596 depolymerization and Rac1 inhibition. *Anim Cells Syst*. 2022;26(6):380–387.

597 24. de Bont JM, et al. Differential expression and prognostic significance of SOX genes in
598 pediatric medulloblastoma and ependymoma identified by microarray analysis. *Neuro-Oncol*.
599 2008;10(5):648–660.

600 25. Hovestadt V, et al. Resolving medulloblastoma cellular architecture by single-cell genomics.
601 *Nature*. 2019;572(7767):74–79.

602 26. Darmanis S, et al. A survey of human brain transcriptome diversity at the single cell level.
603 *Proc Natl Acad Sci*. 2015;112(23):7285–7290.

604 27. Yang F, et al. A Druggable UHRF1/DNMT1/GLI Complex Regulates Sonic Hedgehog–
605 Dependent Tumor Growth. *Mol Cancer Res*. 2022;20(11):1598–1610.

606 28. Goka ET, et al. RAC1b Overexpression Confers Resistance to Chemotherapy Treatment in
607 Colorectal Cancer. *Mol Cancer Ther*. 2019;18(5):957–968.

608 29. Goka ET, et al. Rac Signaling Drives Clear Cell Renal Carcinoma Tumor Growth by Priming
609 the Tumor Microenvironment for an Angiogenic Switch. *Mol Cancer Ther*. 2020;19(7):1462–
610 1473.

611 30. Bailly C, et al. Rac1 as a therapeutic anticancer target: Promises and limitations. *Biochem*
612 *Pharmacol*. 2022;203:115180.

613 31. Sauzeau V, Beignet J, Bailly C. Rac1 as a Target to Treat Dysfunctions and Cancer of the
614 Bladder. *Biomedicines*. 2022;10(6). https://doi.org/10.3390/biomedicines10061357.

615 32. Sun J, et al. RAC1 plays an essential role in estrogen receptor alpha function in breast cancer
616 cells. *Oncogene*. 2021;40(40):5950–5962.

617 33. Barros P, Jordan ,Peter, and Matos P. Rac1 Signaling Modulates BCL-6-Mediated Repression
618 of Gene Transcription. *Mol Cell Biol*. 2009;29(15):4156–4166.

619 34. Buongiorno P, et al. Rac1 GTPase and the Rac1 exchange factor Tiam1 associate with Wnt-
620 responsive promoters to enhance beta-catenin/TCF-dependent transcription in colorectal
621 cancer cells. *Mol Cancer*. 2008;7(1):73.

622 35. Kurdi AT, et al. Tiam1/Rac1 complex controls Il17a transcription and autoimmunity. *Nat*
623 *Commun*. 2016;7(1):13048.

624 36. Goka ET, et al. Rac Signaling Drives Clear Cell Renal Carcinoma Tumor Growth by Priming
625 the Tumor Microenvironment for an Angiogenic Switch. *Mol Cancer Ther*. 2020;19(7):1462–
626 1473.

627 37. Basten SG, Giles RH. Functional aspects of primary cilia in signaling, cell cycle and
628 tumorigenesis. *Cilia*. 2013;2(1):6.

629 38. Youn YH, et al. Primary cilia control translation and the cell cycle in medulloblastoma. *Genes*
630 *Dev*. 2022;36(11–12):737–751.

631 39. Crawford AJ, et al. Tumor proliferation and invasion are intrinsically coupled and unraveled
632 through tunable spheroid and physics-based models. *Acta Biomater*. 2024;175:170–185.

633 40. Yoshida T, et al. Blockade of Rac1 Activity Induces G1 Cell Cycle Arrest or Apoptosis in Breast
634 Cancer Cells through Downregulation of Cyclin D1, Survivin, and X-Linked Inhibitor of Apoptosis
635 Protein. *Mol Cancer Ther*. 2010;9(6):1657–1668.

636 41. Tian S, et al. Inhibition of primary cilia-hedgehog signaling axis triggers autophagic cell death
637 and suppresses malignant progression of VHL wild-type ccRCC. *Cell Death Dis*. 2024;15(10):739.

638 42. Caspary T, Larkins CE, Anderson KV. The Graded Response to Sonic Hedgehog Depends on
639 Cilia Architecture. *Dev Cell*. 2007;12(5):767–778.

640 43. Sun Z, et al. A genetic screen in zebrafish identifies cilia genes as a principal cause of cystic
641 kidney. *Development*. 2004;131(16):4085–4093.

642 44. Rahimi AM, et al. Expression of α-Tubulin Acetyltransferase 1 and Tubulin Acetylation as
643 Selective Forces in Cell Competition. *Cells*. 2021;10(2). https://doi.org/10.3390/cells10020390.

644 45. Navarro-Lérida I, et al. Rac1 Nucleocytoplasmic Shuttling Drives Nuclear Shape Changes and
645 Tumor Invasion. *Dev Cell*. 2015;32(3):318–334.

646 46. Michaelson D, et al. Rac1 accumulates in the nucleus during the G2 phase of the cell cycle
647 and promotes cell division. *J Cell Biol*. 2008;181(3):485–496.

648 47. Epting D, et al. The Rac1 regulator ELMO controls basal body migration and docking in
649 multiciliated cells through interaction with Ezrin. *Development*. 2015;142(1):174–184.

650 48. Del Debbio CB, et al. Rho GTPases Control Ciliary Epithelium Cells Proliferation and
651 Progenitor Profile Induction In Vivo. *Invest Ophthalmol Vis Sci*. 2014;55(4):2631–2641.

652 49. Lee M, et al. Proliferation associated 2G4 is required for the ciliation of vertebrate motile
653 cilia. *Commun Biol*. 2024;7(1):1430.

654 50. Pintado P, et al. Arl13b interferes with α-tubulin acetylation. *Cilia*. 2015;4(1):P73.

655 51. Tsiami F, et al. Genome-wide CRISPR-Cas9 knockout screens identify DNMT1 as a druggable
656 dependency in sonic hedgehog medulloblastoma. *Acta Neuropathol Commun*. 2024;12(1):125.

657 52. Pereira V, et al. Clinical and molecular analysis of smoothened inhibitors in Sonic Hedgehog
658 medulloblastoma. *Neuro-Oncol Adv*. 2021;3(1):vdab097.

659 53. Nellan A, Jackson S. Targeted therapy done right: Direct sonic hedgehog inhibition for sonic
660 hedgehog medulloblastoma. *Neuro-Oncol*. 2024;26(4):623–624.

661 54. Kool M, et al. Genome Sequencing of SHH Medulloblastoma Predicts Genotype-Related
662 Response to Smoothened Inhibition. *Cancer Cell*. 2014;25(3):393–405.

663 55. Zhang Z-Y, et al. Regulation of UHRF1 by microRNA-378 modulates medulloblastoma cell
664 proliferation and apoptosis. *Oncol Rep*. 2017;38(5):3078–3084.

665 56. Wang Y, et al. UHRF1 inhibition epigenetically reprograms cancer stem cells to suppress the
666 tumorigenic phenotype of hepatocellular carcinoma. *Cell Death Dis*. 2023;14(6):381.

667 57. Zhang Z-Y, et al. Clinicopathological analysis of UHRF1 expression in medulloblastoma
668 tissues and its regulation on tumor cell proliferation. *Med Oncol*. 2016;33(9):99.

669 58. Bailly C, et al. Implication of Rac1 GTPase in molecular and cellular mitochondrial functions.
670 *Life Sci*. 2024;342:122510.

671 59. Butler A, et al. Integrating single-cell transcriptomic data across different conditions,
672 technologies, and species. *Nat Biotechnol*. 2018;36(5):411–420.

673 60. Stuart T, et al. Comprehensive Integration of Single-Cell Data. *Cell*. 2019;177(7):1888-
674 1902.e21.

675 61. Hao Y, et al. Dictionary learning for integrative, multimodal and scalable single-cell analysis.
676 *Nat Biotechnol*. 2024;42(2):293–304.

677 62. Hao Y, et al. Integrated analysis of multimodal single-cell data. *Cell*. 2021;184(13):3573-
678 3587.e29.

679 63. Satija R, et al. Spatial reconstruction of single-cell gene expression data. *Nat Biotechnol*.
680 2015;33(5):495–502.

681 64. Finak G, et al. MAST: a flexible statistical framework for assessing transcriptional changes
682 and characterizing heterogeneity in single-cell RNA sequencing data. *Genome Biol*.
683 2015;16(1):278.

684 65. Bowman RL, et al. GlioVis data portal for visualization and analysis of brain tumor
685 expression datasets. *Neuro-Oncol*. 2017;19(1):139–141.

686 66. Rodriguez-Blanco J, et al. Triptolide and its prodrug Minnelide target high-risk MYC-
687 amplified medulloblastoma in preclinical models. *J Clin Invest*. 2024;134(15).
688 https://doi.org/10.1172/JCI171136.

689 67. Taylor R, et al. Regulation of GLI1 by cis DNA elements and epigenetic marks. *DNA Repair*.
690 2019;79:10–21.

691

692

693

694

695

696

697

698

699

700

701

702

703 **Figure Legends**

704

705 **Figure 1. RAC1 is overexpressed in medulloblastoma tumors relative to normal**
706 **cerebellum.** (A) RAC1 mRNA expression in normal cerebellum and medulloblastoma
707 samples from de Bont et al. 2008 microarray data. (B) RAC1 expression levels in
708 neoplastic and non-neoplastic cell populations based on scRNA-seq analysis of MB
709 tumors and healthy brain tissue. (C) RAC1 expression levels in neoplastic cells versus
710 various non-neoplastic cell types, including oligodendrocytes, microglia, neural,
711 endothelial and astrocytes cells. (D) Representative images and quantification of
712 immunohistochemical staining of human cerebellum, MB tumor, MB lung metastasis, and
713 MB bone metastasis for RAC1 (means ±SD, different fields of cerebellum n=2, MB n=3,
714 lung n=1, bone n=1, p values by unpaired 2-tailed t-Test *P<0.05, **P<0.001,
715 ****P<0.0001) (Source data file).

716

717 **Figure 2. RAC1 depletion in Shh-MB cells reduces levels of GLI1, GLI2, DNMT1 and**
718 **UHRF1.** (A-D) Representative immunoblots for RAC1, GLI1, GLI2, DNMT1 and UHRF1
719 levels, and their corresponding loading control (β Tubulin or β Actin) after Rac1 siRNA

720 mediated depletion in ONS76 cells; (means ±SD, n= 3-5, p values by unpaired 2-tailed t-
721 Test *P<0.05, **P<0.001, ****P<0.0001), (E) Relative mRNA expression of RAC1, GLI1,
722 GLI2, DNMT1 and UHRF1 in ONS76 cells (means ±SD, n= 2; p values by unpaired 2-
723 tailed t-Test *P<0.05, **P<0.001, ****P<0.0001) (Source data file).
724
725 **Figure 3. RAC1 inhibition by GYS32661 in Shh-MB cells reduces levels of GLI1,**
726 **GLI2, DNMT1 and UHRF1.** (A) Representative immunoblots showing RAC1-GTP and
727 RAC1 levels with their corresponding loading control (β Tubulin) after treatment with
728 varying GYS32661 concentrations for 24 hours in ONS76 cells. (B) Immunoblot
729 representative images showing GLI1 protein expression in ONS76 cells as compared to
730 its corresponding loading control GAPDH and GLI1, after 8μM, GYS32661 treatment at
731 different time points. (C-D) Immunoblot representative images showing GLI2, UHRF1,
732 and DNMT1 expression as compared to their corresponding loading control (β Actin or
733 GAPDH) in ONS76 cells after GYS32661 treatment at different time points. (E)
734 Representative immunoblots showing GLI1, GLI2 and DNMT1 levels and their
735 corresponding loading control (β Tubulin) after treatment with different concentrations of
736 GYS32661 for 24 hours in MSC4 cells. (F) Representative immunoblots demonstrating
737 UHRF1 levels in MSC4 cells with its corresponding loading control (β Actin) after
738 treatment with different concentrations of GYS32661 for 24 hours. (G) Quantitative
739 representation of relative mRNA levels of GLI1 in ONS76 cells after GYS32661 treatment
740 at different time points (means ±SD, n=2; values by unpaired 2-tailed t-Test *P<0.05,
741 **P<0.001, ****P<0.0001). (H) Quantitative representation of ChIP qPCR of ONS76 cells
742 upon GYS32661 treatment (means ±SD, n=2; values by two-way ANOVA with

743 uncorrected Fisher's LSD, *P<0.05, **P<0.001, ****P<0.0001 representative of 3
744 individual replicates); (I) Diagram representing the binding site of RAC1 at the GLI1
745 upstream promoter region (Source data file).
746
747 **Figure 4. GYS32661 treatment reduces GLI1-GLI2-DNMT1-UHRF1 interactions in**
748 **Shh-MB cells**. (A & B) Representative images of PLA assays of ONS76 and MSC4 cells
749 upon GYS32661 treatment for 24 hours showing the GLI1-DNMT1 interaction, (means
750 ±SD, n= 5-10; values by unpaired 2-tailed t-Test *P<0.05, **P<0.001, ****P<0.0001). (C
751 & D) Representative images of PLA assay of ONS76 and MSC4 cells after GYS32661
752 treatment for 24 hours showing GLI1-UHRF1 interaction (means ±SD, n= 5-10; values by
753 unpaired 2-tailed t-Test *P<0.05, **P<0.001, ****P<0.0001) (Source data file).
754
755 **Figure 5. GYS32661 treatment reduces Shh-MB growth *in vivo***. (A & B)
756 Representative MRI images of Shh-MB tumors after *in vivo* MSC4 cell orthotopic injection
757 after endpoint of the vehicle (Upper images in A) or GYS32661 (Lower images in A)
758 treatment, and their representative H&E images, respectively; (B) Quantitation of tumor
759 volumes of orthotopic MSC4 mouse Shh-MB tumors after the endpoint of GYS32661
760 cohort (means ±SD, n= 12 individual mice per group; values by unpaired 2-tailed t-Test
761 *P<0.05, **P<0.001, ****P<0.0001); (D) Kaplan Meier survival curve analysis of orthotopic
762 MSC4 mouse Shh-MB tumors of GYS32661 cohort (means ±SD, n= 12 individual mice
763 per group). (E & F) Representative IHC images of MSC4 mouse orthotopic Shh-MB
764 tumors after the GYS32661 cohort demonstrating Ki67, Cleaved Caspase-3, GLI1, GLI2
765 and DNMT1 protein levels, respectively; (means ±SD, n=7 different fields of n=4

766 representative individual mice; values by unpaired 2-tailed t-Test *P<0.05, **P<0.001,
767 ****P<0.0001) (Source data file).
768
769 **Graphical abstract: RAC1 controls Shh-MB progression by binding to the GLI1**
770 **promoter.** Graphical abstract demonstrating RAC1 localizes to the nucleus and binds to
771 the GLI1 promoter and plays an important role in its transcription. RAC1 genetic or
772 GYS32661 mediated inhibition leads to RAC1 dissociation from the GLI1 promoter and
773 transcriptional repression of Shh-MB biomarkers GLI2, DNMT1 and UHRF1. This
774 eventually causes inhibition of Shh-MB tumor cell proliferation and migration, which leads
775 to a decrease in Shh-MB development.
776
777
778 **Supplementary Figure S1. ONS76 expresses higher RAC1 than other cancer cells**.
779 Immunoblots showing RAC1 expression in different cancer cells with their corresponding
780 loading control, and quantification (means ±SD, n= 3). Immunoblots shown are
781 representative of 3 individual biological replicates (Source data file).
782
783 **Supplementary Figure S2. GYS32661 is well-tolerated *in vivo* in mice**. (A) Body
784 weight of C57BL/6 mice with intracranial MSC4 cells after GYS32661 treatment.
785 GYS32661 was administered at 35 mg/kg and animals were weighed on days 4, 6, 8, 19,
786 and 12 (means ±SD, n=12 per group). (B-C) Weights of male and female rats after
787 GYS32661 treatment at varying doses for 28 days (means ±SD, n= 20 per group) (Source
788 data file).

789

790 **Supplementary Figure S3. GYS32661 is non-toxic and brain penetrant in rats**. (A-D)
791 Male and female rats received intraperitoneal GYS32661 administration at different doses
792 and organs were harvested after 28 days. Liver and brain weights of male or female were
793 collected after for 28 days (means ± SD, n=20 per group). (E-F) Concentration of
794 GYS32661 in the brain (E) and brain to plasma ratio (F) was measured in mice after 10
795 mg/kg intraperitoneal injection. Measurements were taken at various time intervals post
796 administration (means ± SD, n=2) (Source data file).

797

798 **Supplementary Figure S4. GYS32661 treatment reduces transcription of GLI1,**
799 **components of GLI-UHRF1-DNMT1 complex, and GLI1-GLI2 interaction**. (A)
800 Quantitation of the relative mRNA expression of *Gli1*, *Gli2*, *Dnmt1* and *Uhrf1* in MSC4
801 cells (means ±SD, n=2; p values by unpaired 2-tailed t-Test *P<0.05, **P<0.001,
802 ****P<0.0001). (B) Representative images of ONS76 cells GLI1-GLI2 PLA assay after
803 control and RAC1 siRNA treatment (GLI1-GLI2 PLA:Red; DAPI: Blue) and its quantitative
804 representation (means ±SD, n=5; p values by unpaired 2-tailed t-Test *P<0.05,
805 **P<0.001, ****P<0.0001) (Source data file).

806

807 **Supplementary Figure S5. GYS32661 treatment reduces Shh-MB cell migration *in***
808 ***vitro***. (A) Representative images and quantification of % migration of cells *in vitro* wound
809 healing assay of ONS76 cells to test GYS32661 compound (means ±SD, n=10 different
810 areas; values by 2-tailed Student's t-Test P<0.05, **P<0.001, ****P<0.0001
811 representative of 3 individual biological replicates). (B) Quantitation of accumulated

812 distances traveled by ONS76 cells after GYS32661 treatment in a chemotaxis time lapse
813 imaging experiment (means ±SD, n=60 individual cells; values by 2-tailed Student's t-
814 Test *P<0.05, **P<0.001, ****P<0.0001) (Source data file).
815
816 **Supplementary Figure S6. RAC1 inhibition by GYS32661 in Shh-MB cells induces**
817 **morphological changes and cell cycle arrest.** (A) Representative images of actin
818 polymerization assay of ONS76 cells (Phalloidin: green; Alexa Fluor 488 and GLI1: Red
819 (Alexa Fluor 647) and DAPI (Blue) staining (means ±SD, n=10; values by 2-tailed
820 unpaired t-test P<0.05, **P<0.001, ****P<0.0001; images are representative of 3
821 individual biological replicates). (B) Quantification of propidium iodide-FACS staining of
822 ONS76 cells after GYS32661 treatment at different time points. (C) Immunoblot
823 representative images showing Cyclin D1 expression and its quantitation as compared to
824 loading control (β Actin) in ONS76 cells after GYS32661 treatment at different time points
825 (means ±SD, n=3; values by 2-tailed Student's t-Test P<0.05, **P<0.001, ****P<0.0001)
826 (Source data file).
827
828
829 **Supplementary Figure S7. GYS32661 treatment affects cell proliferation and**
830 **intraciliary signaling in Shh-MB cells *in vitro***. (A) Representative images of ONS76
831 cells show cilia labeled with acetylated tubulin (red) and pericentrium (green) after
832 GYS32661 treatment for 24 hours. Quantitative analysis was performed of cilia and
833 pericentrium (means ±SD, n=3 different areas; values by 2-tailed Student's t-Test P<0.05,
834 **P<0.001, ****P<0.0001 representative of 3 individual biological replicates); (B-C)

835 Representative immunoblots images show Ift88, pGsk3β, Total Gskβ, pVav2, Vav2,
836 pPak1 and Pak1 levels with corresponding loading control (β Actin or GAPDH) after
837 treatment with varying concentrations of GYS32661 for 24 hours in MSC4 cells. (D)
838 Representative immunoblots show Acetylated tubulin (AcTub) and ARL13B expression
839 with corresponding loading control β-Actin after GYS32661 treatment (Source data file).

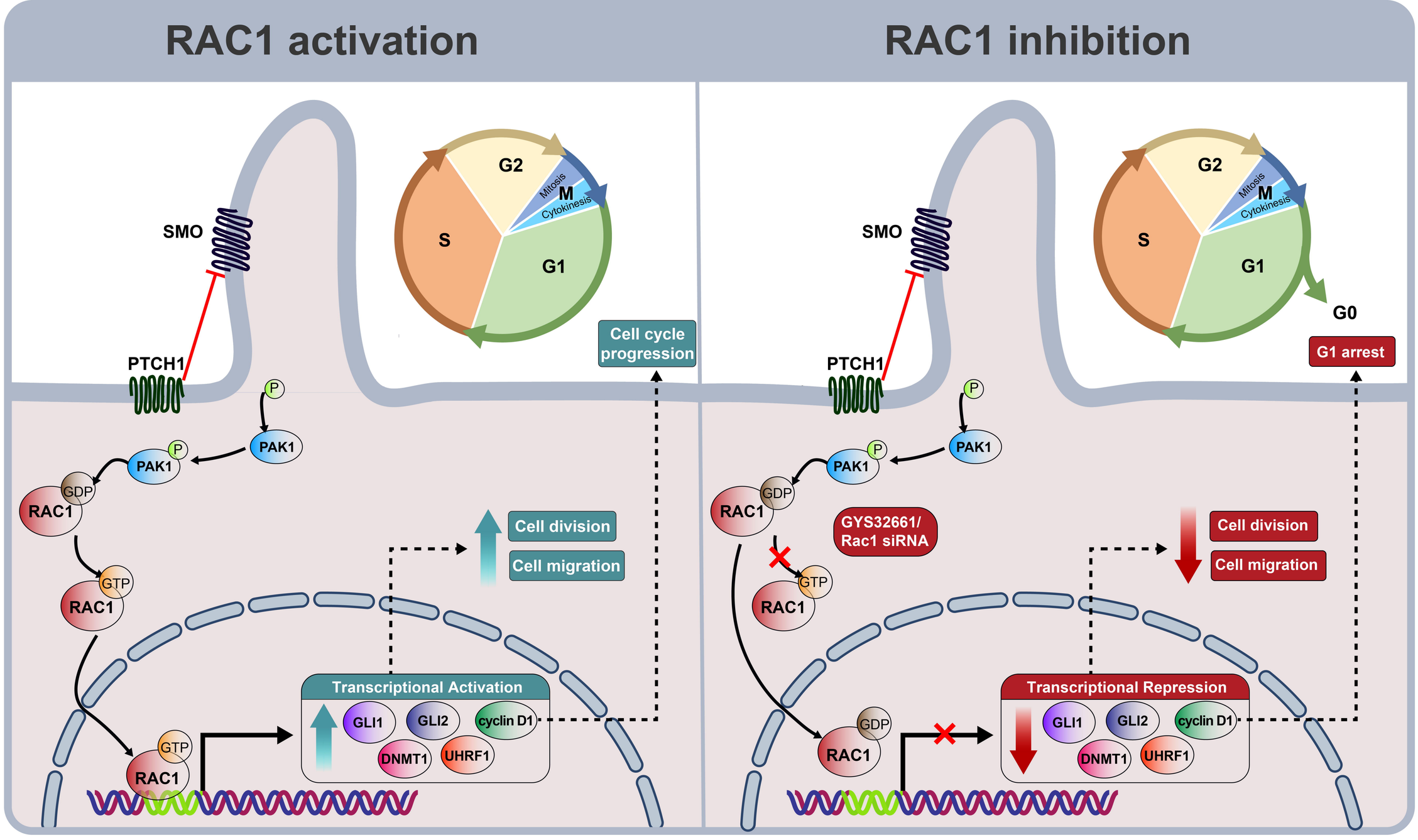
RAC1 activation
RAC1 inhibition
SMO
PTCH1
G2
S
G1
M
Mitosis
Cytokinesis
G0
Cell cycle progression
G1 arrest
P
PAK1
GDP
GTP
RAC1
GYS32661/
Rac1 siRNA
Cell division
Cell migration
Transcriptional Activation
Transcriptional Repression
GLI1
GLI2
cyclin D1
DNMT1
UHRF1

Figure 1

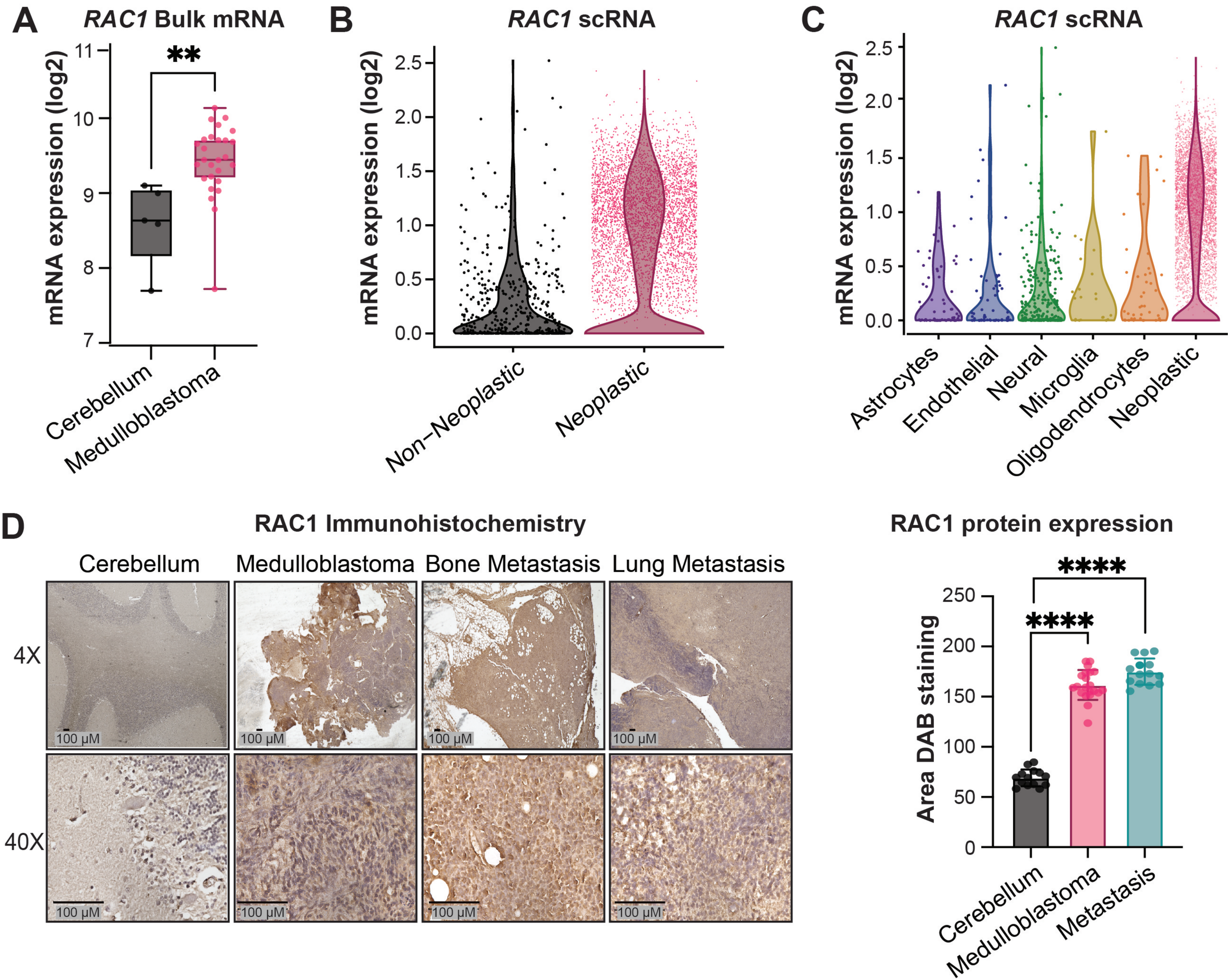
A
RAC1 Bulk mRNA
mRNA expression (log2)
**
Cerebellum
Medulloblastoma
B
RAC1 scRNA
mRNA expression (log2)
Non−Neoplastic
Neoplastic
C
RAC1 scRNA
mRNA expression (log2)
Astrocytes
Endothelial
Neural
Microglia
Oligodendrocytes
Neoplastic
D
RAC1 Immunohistochemistry
Cerebellum
Medulloblastoma
Bone Metastasis
Lung Metastasis
4X
40X
100 µM
RAC1 protein expression
Area DAB staining
****
****
Cerebellum
Medulloblastoma
Metastasis

Figure 2

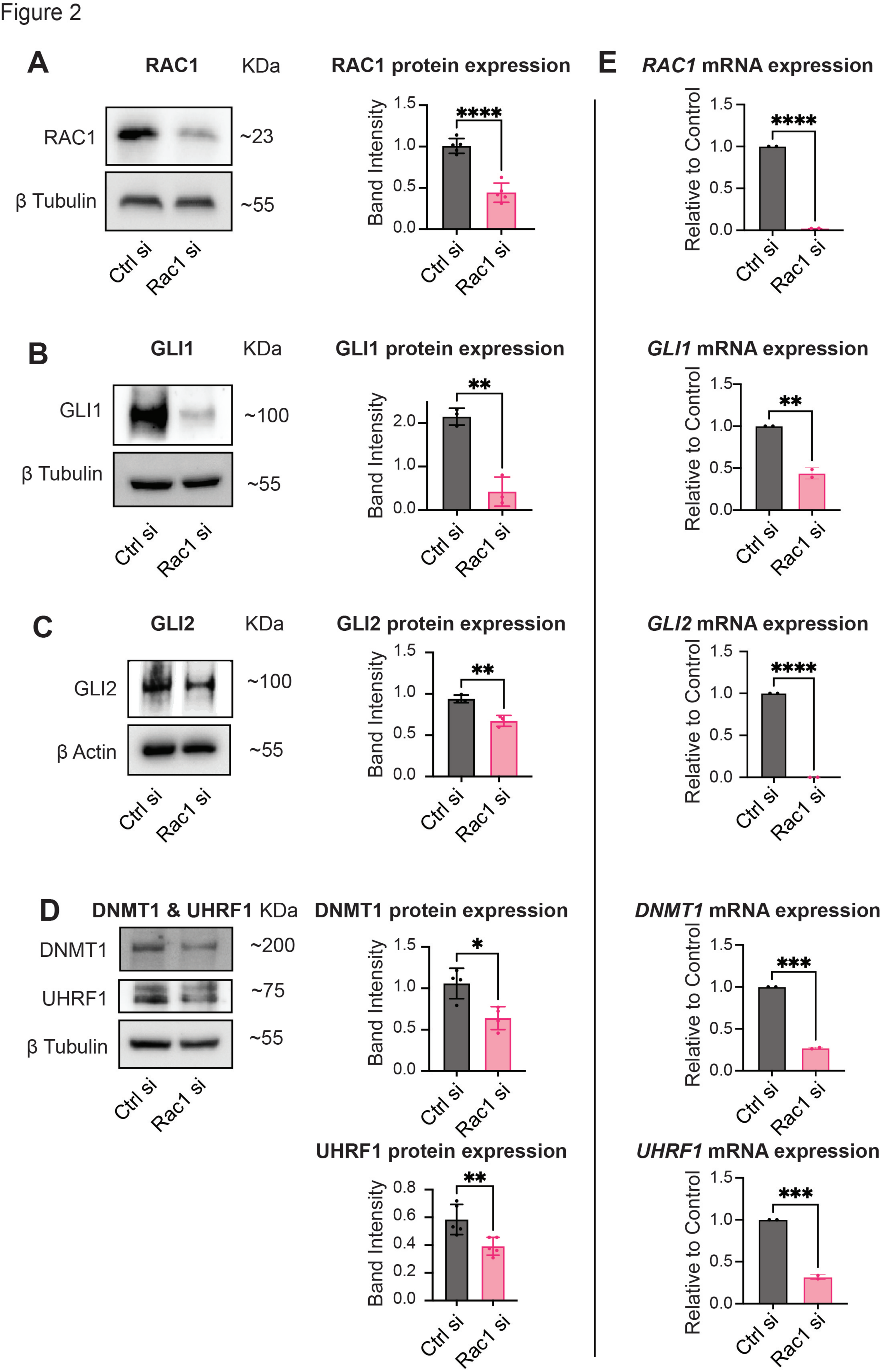
A
RAC1
KDa
RAC1
~23
β Tubulin
~55
Ctrl si
Rac1 si
RAC1 protein expression
Band Intensity
1.5
1.0
0.5
0.0
****
Ctrl si
Rac1 si
E
RAC1 mRNA expression
Relative to Control
1.5
1.0
0.5
0.0
****
Ctrl si
Rac1 si
B
GLI1
KDa
GLI1
~100
β Tubulin
~55
Ctrl si
Rac1 si
GLI1 protein expression
Band Intensity
2.0
1.0
0.0
**
Ctrl si
Rac1 si
GLI1 mRNA expression
Relative to Control
1.5
1.0
0.5
0.0
**
Ctrl si
Rac1 si
C
GLI2
KDa
GLI2
~100
β Actin
~55
Ctrl si
Rac1 si
GLI2 protein expression
Band Intensity
1.5
1.0
0.5
0.0
**
Ctrl si
Rac1 si
GLI2 mRNA expression
Relative to Control
1.5
1.0
0.5
0.0
****
Ctrl si
Rac1 si
D
DNMT1 & UHRF1
KDa
DNMT1
~200
UHRF1
~75
β Tubulin
~55
Ctrl si
Rac1 si
DNMT1 protein expression
Band Intensity
1.5
1.0
0.5
0.0
*
Ctrl si
Rac1 si
DNMT1 mRNA expression
Relative to Control
1.5
1.0
0.5
0.0
***
Ctrl si
Rac1 si
UHRF1 protein expression
Band Intensity
0.8
0.6
0.4
0.2
0.0
**
Ctrl si
Rac1 si
UHRF1 mRNA expression
Relative to Control
1.5
1.0
0.5
0.0
***
Ctrl si
Rac1 si

Figure 3

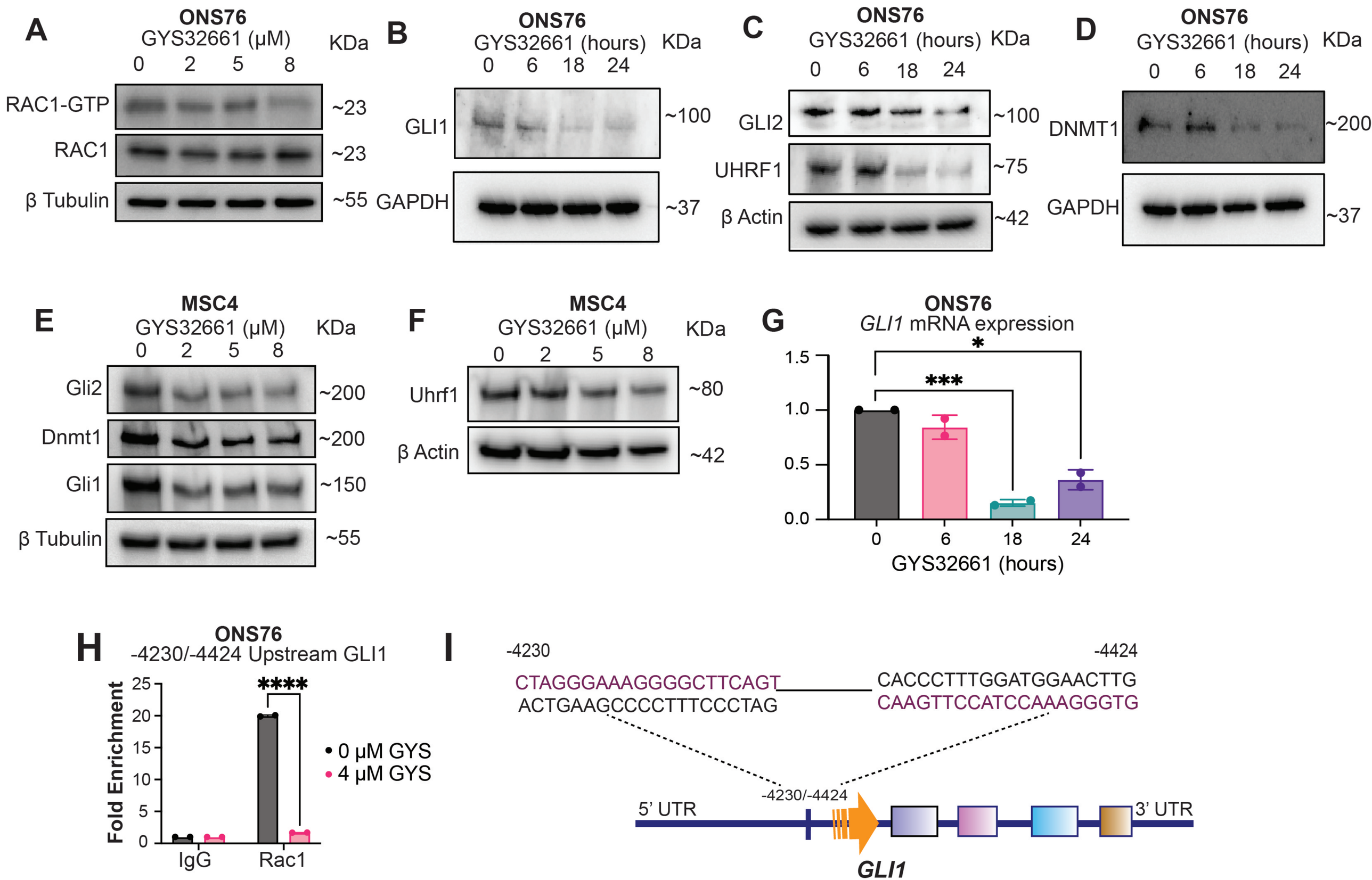
A
ONS76
GYS32661 (μM)
0 2 5 8
KDa
RAC1-GTP
RAC1
β Tubulin
~23
~23
~55
B
ONS76
GYS32661 (hours)
0 6 18 24
KDa
GLI1
GAPDH
~100
~37
C
ONS76
GYS32661 (hours)
0 6 18 24
KDa
GLI2
UHRF1
β Actin
~100
~75
~42
D
ONS76
GYS32661 (hours)
0 6 18 24
KDa
DNMT1
GAPDH
~200
~37
E
MSC4
GYS32661 (μM)
0 2 5 8
KDa
Gli2
Dnmt1
Gli1
β Tubulin
~200
~200
~150
~55
F
MSC4
GYS32661 (μM)
0 2 5 8
KDa
Uhrf1
β Actin
~80
~42
G
ONS76
GLI1 mRNA expression
*
***
1.5
1.0
0.5
0.0
0 6 18 24
GYS32661 (hours)
H
ONS76
-4230/-4424 Upstream GLI1
****
Fold Enrichment
25
20
15
10
5
0
IgG
Rac1
0 μM GYS
4 μM GYS
I
-4230
-4424
CTAGGGAAAGGGGCTTCAGT
ACTGAAGCCCCTTTCCCTAG
CACCCTTTGGATGGAACTTG
CAAGTTCCATCCAAAGGGTG
-4230/-4424
5' UTR
3' UTR
GLI1

Figure 4

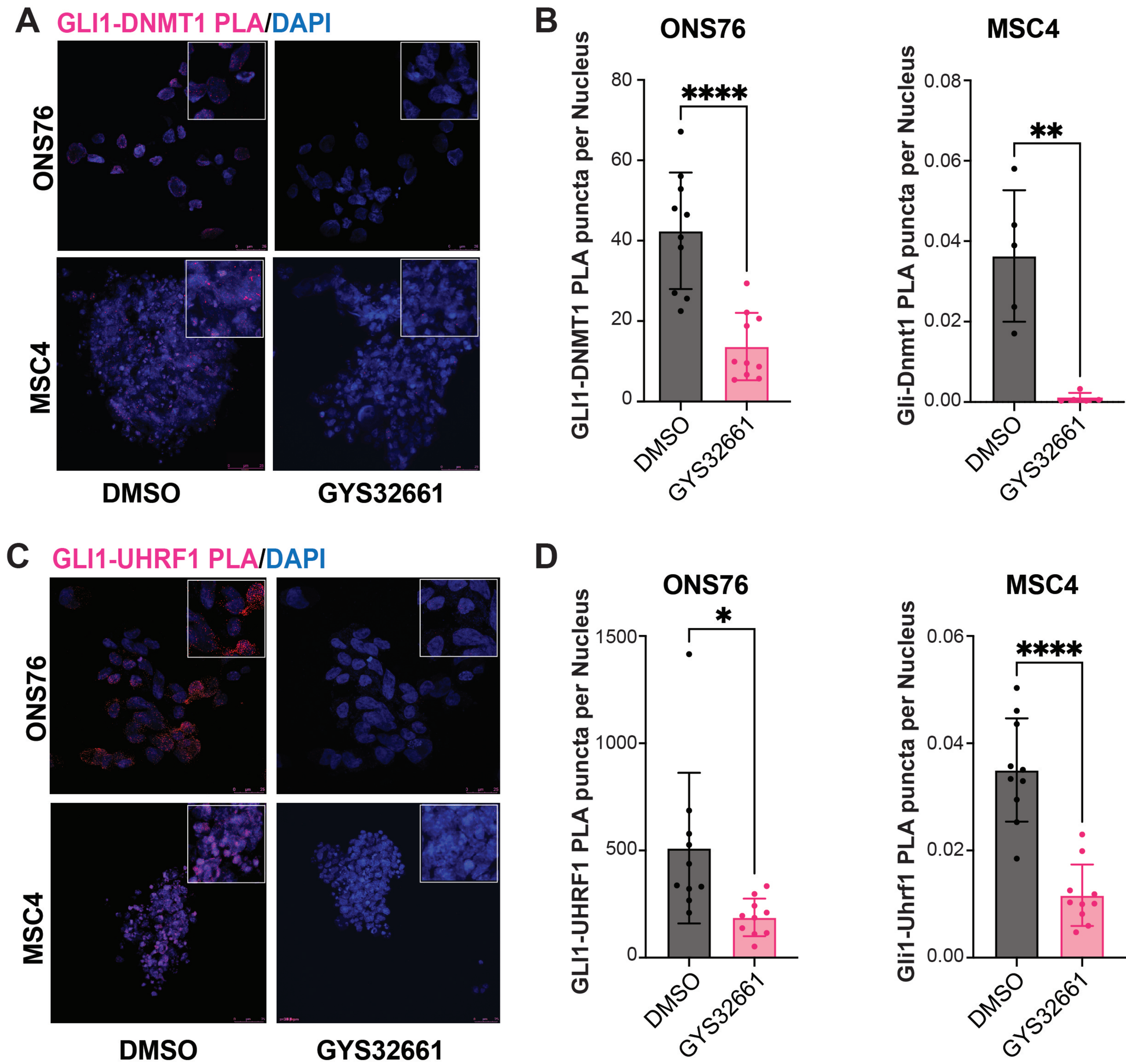
A
GLI1-DNMT1 PLA/DAPI
ONS76
MSC4
DMSO
GYS32661
B
ONS76
GLI1-DNMT1 PLA puncta per Nucleus
80
60
40
20
0
****
DMSO
GYS32661
MSC4
Gli-Dnmt1 PLA puncta per Nucleus
0.08
0.06
0.04
0.02
0.00
**
DMSO
GYS32661
C
GLI1-UHRF1 PLA/DAPI
ONS76
MSC4
DMSO
GYS32661
D
ONS76
GLI1-UHRF1 PLA puncta per Nucleus
1500
1000
500
0
*
DMSO
GYS32661
MSC4
Gli1-Uhrf1 PLA puncta per Nucleus
0.06
0.04
0.02
0.00
****
DMSO
GYS32661

Figure 5

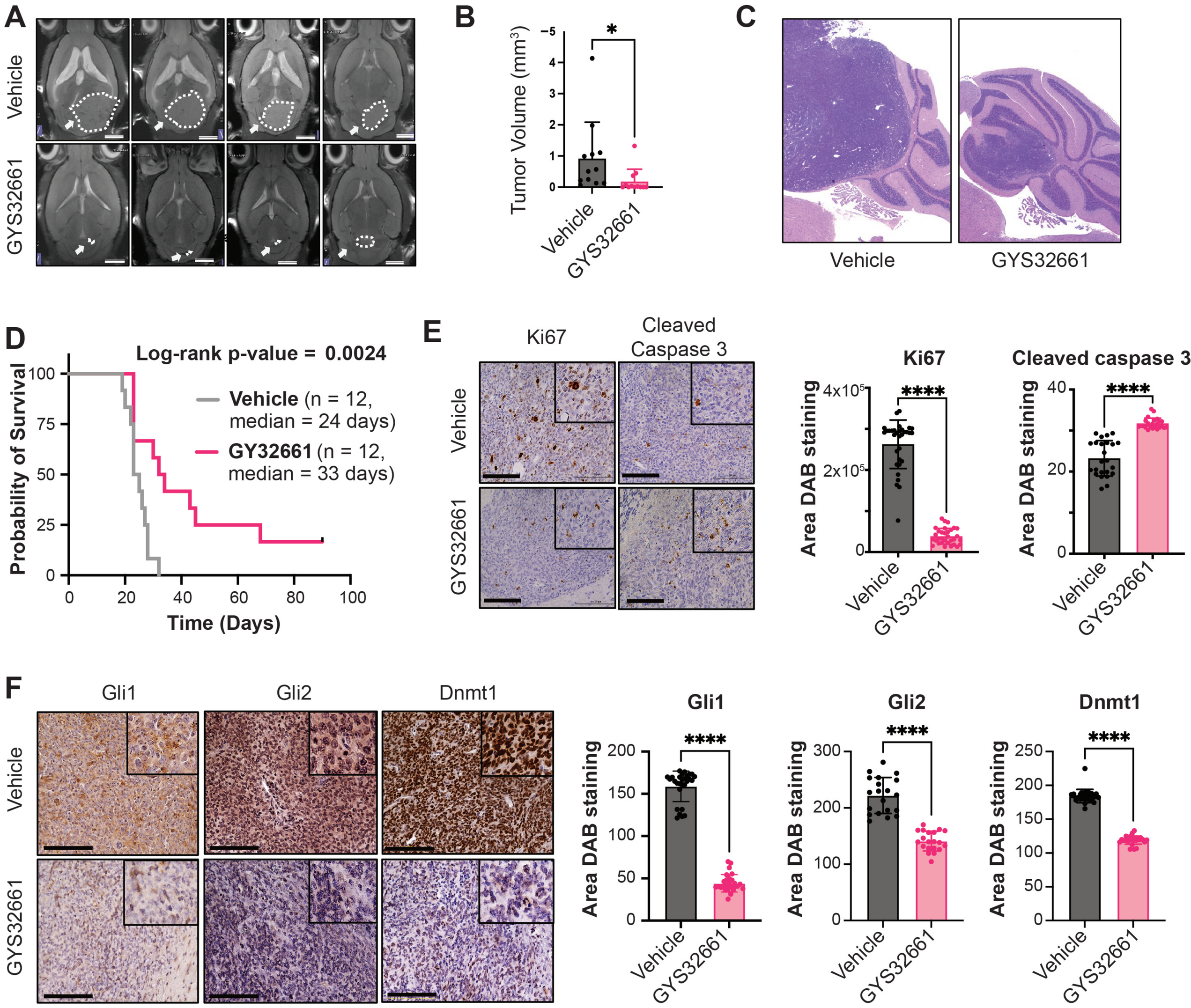
A
Vehicle
GYS32661
B
Tumor Volume (mm3)
*
Vehicle
GYS32661
C
Vehicle
GYS32661
D
Log-rank p-value = 0.0024
Probability of Survival
Vehicle (n = 12, median = 24 days)
GY32661 (n = 12, median = 33 days)
Time (Days)
E
Ki67
Cleaved Caspase 3
Vehicle
GYS32661
Ki67
Cleaved caspase 3
Area DAB staining
****
Vehicle
GYS32661
F
Gli1
Gli2
Dnmt1
Vehicle
GYS32661
Gli1
Gli2
Dnmt1
Area DAB staining
****
Vehicle
GYS32661